Study of Photodegradation Performance and Ability of Lead Removal of Synthesized Maghemite Nanoparticles Using Ziziphus Jujuba Extract

Abdolhossein Miri
Zabol University of Medical Sciences
Atefeh Sadat Sedighi
Zabol University of Medical Sciences
Ahmad Najafidoust
Sahand University of Technology
Mehrdad Khatami
Bam University of Medical Sciences
Mina sarani (minasarani64@gmail.com)
Zabol University of Medical Sciences https://orcid.org/0000-0002-0681-0421

Research Article

Keywords: γ-Fe2O3 NPs, Ziziphus jujuba, Lead removal, Photocatalytic Activity, Green chemistry

Posted Date: May 27th, 2021

DOI: https://doi.org/10.21203/rs.3.rs-545585/v1

Abstract

Today, Water pollutants such as heavy metals and dyes are very important dangers to the nature. Metals such as lead, chromium, mercury and arsenic are examples of heavy metals which are toxic to living things, even sometime at the lowest concentrations. For resolve this challenge, Magnetic nanoparticles are attractive compound because of their advantages such as high efficiency, fast recovery capability, high surface area, easy transportation and inexpensive. We presented an easy and eco-friendly route for the synthesis of iron oxide nanoparticles using *Ziziphus jujuba* extract. In order to determine the physical, chemical and optical properties of the synthesized samples, Fourier-transform infrared (FT-IR), powder X-ray diffraction (PXRD), vibrating sample magnetometer (VSM), field emission scanning electron microscope (FESEM), energy dispersive X-ray (EDX), transmission electron microscopy (TEM), and Raman analyses were deployed. PXRD results showed that the synthesized nanoparticles have maghemite form of (γ-Fe_2O_3). FESEM and TEM results demonstrated that the size of these nanoparticles was in range of 20-50 nm, and had spherical shapes. Raman spectrum confirmed the cubic structure of γ-Fe_2O_3 NPs. Survey of magnetic properties showed that the synthesized maghemite nanoparticles (γ-Fe_2O_3 NPs) were superparamagnetic. The ability to remove lead from aqueous solution was investigated using these nanoparticles. The results showed that the synthesized nanoparticles were capable of removing 96% of lead at pH = 7 and 1 mg/L loading of nanoparticles. The photocatalytic activity of γ-Fe_2O_3 NPs was studied on methylene blue (MB) dye; as a result, MB at pH =7 and 1 gr dosage of γ-Fe_2O_3 had the highest removal percentage (92.8%) during 160 minute using γ-Fe_2O_3 which calcined at 400 ˚C. The reusability results showed that after four cycles of using the γ-Fe_2O_3-400, the obtained degradation of methylene blue was about 87.1%. Thus, synthesized γ-Fe_2O_3 NPs can be a good alternative for removing heavy metals and industrial dyes from contaminated waters.

Introduction

Generally, iron oxide is a chemical compound containing iron and oxygen, and is widely available in nature and has attracted much attention due to its various oxidation states [1]. Iron oxide can be utilized in industries as catalysts, pigments, sensors; heavy metal contaminates removal agents, and bacteria-killing materials. It was also explored in clinical trials as a targeted drug delivery system for cancer therapy [2,4-7]. Due to the ability and widespread applications of iron oxide nanoparticles, much attention has been paid to the synthesis of well-organized nanoparticles with unique sizes and morphologies. Indeed, by decreasing the size of particles, their surface activities were also increased. Chemical and physical synthesis methods such as co-precipitation [8], hydrothermal [9], solvothermal [10,11] and microemulsion [12] were deployed for the preparation of iron oxide nanoparticles; but today due to the low toxicity, cheapness, availability, high efficiency and environmentally friendly properties, natural metabolites and resources have been utilized to synthesize these nanoparticles with unique features [3-5,13-15].

Water pollutants such as heavy metals and dyes are very important dangers to the nature. Metals such as lead, chromium, mercury and arsenic are examples of heavy metals which are toxic to living things, even sometime at the lowest concentrations [16]. The risk of contamination of water by paint compounds threatens aquatic life; additionally, it can raise the risk of cancer in humans. Due to the environmental hazards and toxic health effects of heavy metals and dyes, various technologies such as chemical precipitation, ion exchange, and adsorption have been developed to remove them [17,18]. Magnetic nanoparticles are attractive compound because of their advantages such as high efficiency, fast recovery capability, high surface area, easy transportation and inexpensive [19]. Sun *et al* have synthesized Fe_3O_4@SiO_2-NH_2 nanoparticles and evaluated their capabilities for removing green malachite dye. Their results showed high efficiency for the elimination of green malachite using the modified magnetite [20].

Ziziphus jujuba (from the family of Rhamnaceae) grows in tropical regions, parts of India and Myanmar. Its fruit contains many compounds including saponins, alkaloids, flavonoids, terpenoids, glycosides, ascorbic acid, thiamine, riboflavin-bioflavonoids and pectin. Due to the invaluable ingredients of *Z. jujube*, it can be expected that its extract is able to reduce and stabilize iron salts [21]. Therefore, in this study, iron oxide nanoparticles (γ-Fe_2O_3 NPs) were synthesized using aqueous extract of *Z. jujuba* fruit, and their efficacy as adsorbents for removing lead from aqueous solutions as well as their photocatalytic activity are investigated.

Experiments

Extraction of Z. jujuba

Dried *Z. jujuba* fruit was bought from Birjand. Then, kernels were separated from the fruit, and reside was powder. 20 mL of distilled water was added to 2 gr of *Z. jujube* power. The mixture was shacked for 24 hours at 150 rpm, and the result was filtered using filter paper of Whatman® No.1; the filtrate was utilized for additional experimental procedures.

Synthesis of γ-Fe_2O_3 NPs

To synthesize nanoparticles, 90 mL of distilled water was poured to the 10 mL of *Z. jujube* extract. The solution was gradually added to 100 mL of iron (III) chloride (0.1 M) solution. The final solution was stirred in a water bath at 70 ˚C (about 3 hours). The pH of reaction was tuned 11 using sodium hydroxide (1 M) solutions. Result was dark brown solution that dried in the oven at 90 ˚C. The resulting powder was calcined separately at 300, 400, and 500 ˚C for about 2 hours, using furnace; the obtained iron oxide nanoparticles were brown in color and the schematic diagram is depicted in Fig. 1.

Lead removal evaluations

Aqueous solution of lead nitrate (II) was prepared with serials dilutions of 500, 250, 125, 62.5, 31.25 and 15.625 mg/L, and its adsorption was evaluated using atomic adsorption. The pH of 4, 6 and 8 was applied for each dilutions using NaOH (1M) and HCl (1M) solutions. 10 mg of iron oxide nanoparticles

was added to each dilution and well mixed using shaker at 150 rpm for 60 min; finally, the mixture was filtered and the filature adsorption was read using atomic adsorption device.

Photocatalytic performance of γ-Fe_2O_3 NPs

Semi-batch reactor was utilized to evaluate the photocatalytic activity of nanoparticles. In this study, samples were dispersed in heterogeneous form in organic pollutant of methylene blue. The reactor with the photocatalyst was placed in the dark on stirrer for 60 minutes to equilibrium the adsorption-desorption. Additionally, a halogen lamp with a wavelength of visible light was employed as a radiation source. After adsorption-desorption equilibrium, the lamp was turned on, and the solution was exposed to visible light. Samples were taken at 20 min intervals and were centrifuged; and the absorption was read using a UV-Vis spectrophotometer (DR6000) at 665 nm. Degradation efficiency was calculated using the Eq. 1.

$$\text{Degradation effiency}\,\% = (1 - C/C_0) \times 100\% \qquad \text{Eq. 1}$$

Which C_0 is the initial concentration of the organic dye in water, and C is final concentration of dye in the solution in specified times after irradiation.

Characterization

Structure, morphology and size of the synthesized γ-Fe_2O_3 NPs were identified through Raman (Takram P50C0R10 model in 532 nm leaser wave length), Powder X-ray diffraction (PXRD, X'Pert PRO MPD PANalytical model, Netherlands), Fourier transform infrared spectroscopy (FT-IR, Bruker Tensor27) and field energy scanning electron microscopy (FESEM, TESCAN model of MIRA3) methods.

Results And Discussion

Among the nanoparticles with commercial applications, iron oxide nanoparticles have unique properties with abundant applications. Thus, in this study, maghemite nanoparticles (γ-Fe_2O_3 NPs) were synthesized using aqueous solution of *Z. jujube* through simple and fast route with high efficiency.

PXRD analysis

PXRD is one of the efficient devices for materials analysis. The nature and size of particles were characterized using PXRD technique and the resulted patterns [9]. PXRD spectra of the γ-Fe_2O_3 NPs at 300, 400, and 500 ˚C are demonstrated in Fig. 2. In PXRD spectra, sharp peaks indicated the stability of nanoparticles. The high intensity of the peaks indicated strong scattering centers of X-ray in the crystalline phase. Generally, broadening of peaks in PXRD patterns of solid material can be attributed to particle size; wider PXRD peak indicated smaller particle sizes. Additionally, the sharpness of peaks implied the crystallinity of synthesized samples. According to the results obtained from PXRD, Miller

indices of (220), (311), (400), (422), (511), (440) and (533) implied that synthesized samples are maghemite nanoparticles (γ-Fe_2O_3 NPs) with cubic structure (JCPDS: 39-1346) [22]. The crystallite size of these nanoparticles was calculated using the Debye-Scherrer equation (Equation 2).

$D = k\lambda / \beta \cos\theta$ Eq. 2

Where, D is particle size on nanometer, k is a fixed factor that is usually k=1, λ is wavelength of X-ray (3.54 Å), θ is radiation angle of X-ray (in degrees), and β is peak width in half height of the peak that be expressed in units of length [23]. The crystallite size of synthesized γ-Fe_2O_3 nanoparticles at 300, 400, and 500 ˚C were estimated at 28.39, 36.81, and 45.72 nm, respectively.

FESEM and TEM analysis

Analysis of FE-SEM for synthesized γ-Fe_2O_3 nanoparticles exhibited the round-shaped morphology of nanoparticles. The size ranges for synthesized γ-Fe_2O_3 NPs at 300, 400, 500 ˚C were 20-25, ~35, and ~45 nm, respectively (Fig. 3), which were well-surrounded by the respective green coating. The images confirmed that these natural product-based nanoparticles had spherical shapes. The TEM image of synthesized γ-Fe_2O_3 NPs at 400 ˚C showed in Fig. 3, which this figure has been depicted the particles about 40-50 nm sizes with spherical and almost uniform shapes.

FT-IR analysis

The FT-IR spectra of synthesized γ-Fe_2O_3 NPs at 300, 400, and 500 ˚C are shown in Fig. 4. In the FT-IR spectra, the absorption band in range 3414 cm^{-1} caused strong stretching vibration by created hydrogen bonding with OH groups, which absorbed by sample from medium. The absorption band in the range of 1624 cm^{-1} belongs to the adsorbed H_2O groups on the nanoparticle surface. The presence of these peaks indicated that iron oxide nanoparticles are capable of absorbing large amounts of OH groups of H_2O on their outer surfaces. The absorption band in the range of 619-500 cm^{-1} corresponds to the vibration bands O-Fe-O and Fe-O [22,24].

Raman analysis

The Raman spectrum of the synthesized maghemite nanoparticles using aqueous extract of *Z. jujube* at 400 ˚C are shown in Fig. 5. The Raman modes of cubic spinal structures had five active modes including $A_1 + E + 3T_1$. In the region of 286, 687 and 716 cm^{-1}, which are according to A_1, E and T_1 modes, respectively. Raman spectrum confirmed the cubic structure of γ-Fe_2O_3 NPs [25].

VSM analysis

The magnetic properties of the synthesized maghemite nanoparticles at 400 ˚C were investigated using the VSM technique (Fig. 6). Iron nanoparticles had no hysteresis ring and were superparamagnetic at room temperature. The saturation magnetization (Ms) at 400 ˚C was 65 emu/g, which was less than the

magnetic state of its bulk (M_s = 76 emu/g) [26]. This decrease in saturation might be due to the effect of the reduced particle size.

The survey of ability of lead removes

Studies demonstrated that iron oxide nanoparticles were able to remove contaminants. Thus, in this study, the ability of nanoparticles to remove lead was investigated. To evaluate the effect of pH on nanoparticle synthesis, three pHs including 4, 6, and 8 were considered. Based on the results, the pH optimum exhibited that alkaline ambiance was the best condition for the removal of lead. Considering that, the surface charge of γ-Fe_2O_3 NPs can play the most important role in this phenomenon; alkaline ambiance improves the surface charge of nanoparticles [7]. Therefore, the adsorption of lead ions in alkaline ambiance was more than in neutral and acidic ambiance.

In this test, other variables such as contact time and concentration of the synthesized γ-Fe_2O_3 NPs (at 400 ˚C) were considered constantly, and the ability of nanoparticles to remove lead was investigated at 7.90 to 500 mg/L concentrations of pollutants. Lead solution without nanoparticles was considered as a control. The adsorption efficiency was calculated using equation 3.

$R = (C_i - C_e/C_i) \times 100$ Eq. 3

Where, C_i is the initial concentration of lead in solution (mg/L), C_e is equilibrium concentration of lead in solution after adsorption process (mg/L), and R is absorption efficiency. Residual concentrations of lead in solution after adsorption process were calculated by the obtained line equation in Fig. 7A; and by using the obtained results, the adsorption efficiency of lead via the synthesized γ-Fe_2O_3 nanoparticles at 400 ˚C was calculated (Fig. 7B).

Fig. 7B shows that by decreasing the concentrations of lead in the reaction ambiance, the lead removal by nanoparticles was successfully completed. The ratio of 1:1 between the concentration of nanoparticles and lead showed the highest absorption efficiency. As a result, γ-Fe_2O_3 NPs were able to remove lead.

Photocatalytic activity evaluations

Methylene blue degradation

Fig. 8A shows the adsorption diagram of methylene blue dye by the synthetized nanoparticles at 300, 400, and 500 ˚C calcination temperatures. In order to investigate the photocatalytic activity of obtained samples, the applied test condition included pH= 7, 1 g/L of catalyst and 20 mg/L of initial dye concentration. The adsorption of organic dyes using photocatalysts method is directly related to the specific surface area of the photocatalysts. In Fig. 8A, the absorption rate of γ-Fe_2O_3 NPs at 300, 400, and 500 ˚C were 18.2, 20.3, and 16.3%, respectively, which demonstrated that the adsorption rate synthesized sample at 400 ˚C was higher than other samples. Fig. 8B demonstrates that the degradation rate for γ-

Fe_2O_3 NPs at 300, 400, and 500 ˚C were 84.8%, 92.8%, and 70.2%, respectively. According to XRD and FESEM results, by increasing the calcination temperature from 300 ˚C to 500 ˚C, the crystal size was also increased. In photocatalytic activity, ratio of surface-to-volume have role importance than to crystallite size of particles. So, the ratio of surface-to-volume of synthesized nanoparticles at 400 ˚C is higher than to samples of 300 ˚C [27,28], in results, the synthesized nanoparticles at 400 ˚C were exhibited better photocatalytic performances. In sample of 500 ˚C, degradation activity was reduced due to saturation of active sites.

Influence of pH

pH is one of the most effective operational parameters in the photocatalytic process. Given that pH of solution changes the surface charge of nanocatalyst, it has a great influence between the dye molecules and electric charge of photocatalytic. Thus, finding the right amount of pH parameter is essential to increase the removal efficiency [29]. In order to find the optimal pH, the photocatalytic analyses were performed in three different values of 3, 7 and 11. Fig. 9 demonstrates that the removal efficiency of MB dye at pH ranges of 3, 7 and 10 were about 44.9%, 89.1% and 95.8%, respectively. The results exhibited that γ-Fe_2O_3 NPs (at 400 ˚C) had good photocatalytic activity at basic and natural media.

Reusability study

Reusability of photocatalytic is a very important and decisive factor for practical applications. To investigate the stability of synthesized γ-Fe_2O_3 NPs at 400 ˚C, they were exposed to solar light at initial concentrations of 20 mg/L of methylene blue, 1 g/L of catalyst loading and pH = 7 for 160 minutes. After each photocatalytic test, γ-Fe_2O_3 NPs was separated, washed and dried in an oven at 110 ˚C for about 2 hours. The results showed that after four cycles of using the γ-Fe_2O_3-300, the obtained degradation of methylene blue was about 87.1% (Fig. 10). It appears that γ-Fe_2O_3 NPs can be considered as reusable, functional and active of nanophotocatalysts in environmental applications.

Conclusions

In this study, maghemite nanoparticles (γ-Fe_2O_3 NPs) were green-synthesized at 300, 400, and 500 ˚C calcination temperatures using aqueous extract of *Z. jujuba* fruit. The synthesized nanoparticles had a particle size in range of about 20-50 nm. According to the PXRD and FESEM analyses, the calcined sample at 300 ˚C had the lowest particle and crystal size. By increasing calcination temperature, the particle size was also increased. The ability of the green-fabricated nanoparticles to remove lead from the aqueous medium was studied. The removal efficiency of γ-Fe_2O_3 NPs indicated the excellent ability of them to remove lead. Additionally, the study of photocatalytic activity of these nanoparticles at 400 ˚C demonstrated their promising potentials in degradation/removal of MB dye. It can be noted that the number of active sites at the surface of catalysts is high and leads to the increased photocatalytic

activity. Thus, the synthesized γ-Fe_2O_3 NPs can be a good alternative for removing heavy metals and industrial dyes from the contaminated waters.

Declarations

Disclosure statement

The authors declare that they have no competing interests.

References

1. Khan I, Saeed K, Khan I (2019) Nanoparticles: Properties, applications and toxicities. Arab J Chem 12:908–931
2. Ali A, Hira Zafar MZ, ul Haq I, Phull AR, Ali JS, Hussain A (2016) Synthesis, characterization, applications, and challenges of iron oxide nanoparticles. Sci Appl 9:49
3. Miri A, Najafzadeh H, Darroudi M, Miri MJ, Kouhbanani MAJ, Sarani M (2021) Iron Oxide Nanoparticles: Biosynthesis, Magnetic Behavior, Cytotoxic Effect. ChemistryOpen 10:327
4. Khatami M, Alijani HQ, Haghighat M, Bamrovat M, Azhdari S, Ahmadian M, Nobre M, Heidari M, Sarani M, Khatami S (2019) Green Synthesis of Amorphous Iron Oxide Nanoparticles and their Antimicrobial Activity against Klebsiella pneumonia, Pseudomonas aeruginosa and Escherichia coli. Iran J Biotechnol 10:33–39
5. Miri A, Khatami M, Sarani M (2020) Biosynthesis, magnetic and cytotoxic studies of hematite nanoparticles. J Inorg Organomet Polym Mater 30:767–774
6. Lombardo D, Kiselev MA, Caccamo MT (2019) Smart nanoparticles for drug delivery application: development of versatile nanocarrier platforms in biotechnology and nanomedicine. J Nanomater 2019
7. Popescu RC, Savu D, Dorobantu I, Vasile BS, Hosser H, Boldeiu A, Temelie M, Straticiuc M, Iancu DA, Andronescu E, Wenz F, Giordano FA, Herskind C, Veldwijk MR (2020) Efficient uptake and retention of iron oxide-based nanoparticles in HeLa cells leads to an effective intracellular delivery of doxorubicin. Sci Rep 10:10530
8. Besenhard MO, LaGrow AP, Hodzic A, Kriechbaum M, Panariello L, Bais G, Loizou K, Damilos S, Cruz MM, Thanh NTK (2020) Co-precipitation synthesis of stable iron oxide nanoparticles with NaOH: New insights and continuous production via flow chemistry. J Phys Chem C 399:125740
9. Ge S, Shi X, Sun K, Li C, Uher C, Baker JR Jr, Banaszak Holl MM, Orr BG (2009) Facile hydrothermal synthesis of iron oxide nanoparticles with tunable magnetic properties. J Phys Chem C 113:13593–13599
10. Li S, Zhang T, Tang R, Qiu H, Wang C, Zhou Z (2015) Solvothermal synthesis and characterization of monodisperse superparamagnetic iron oxide nanoparticles. J Magn Magn Mater 379:226–231

11. Chen Y, Zhang J, Wang Z, Zhou Z (2019) Solvothermal synthesis of size-controlled monodispersed superparamagnetic iron oxide nanoparticles. Appl Sci 9:5157
12. Chin AB, Yaacob II (2007) Synthesis and characterization of magnetic iron oxide nanoparticles via w/o microemulsion and Massart's procedure. J Mater Proc Technol 191:235–237
13. Azhdari S, Sarabi RE, Rezaeizade N, Mosazade F, Heidari M, Borhani F, Abdollahpour-Alitappeh M, Khatami M (2020) Metallic SPIONP/AgNP synthesis using a novel natural source and their antifungal activities. Rsc Adv 10:29737–29744
14. Hooshmand S, Hayat SMG, Ghorbani A, Khatami M, Pakravanan K, Darroudi M (2020) Preparation and Applications of Superparamagnetic Iron Oxide Nanoparticles in Novel Drug Delivery Systems: An Overview Article. Curr Med Chem
15. Hamidian K, Najafidoust A, Miri A, Sarani M (2021) Photocatalytic performance on degradation of Acid Orange 7 dye using biosynthesized un-doped and Co doped CeO_2 nanoparticles. Mater Res Bull 138:111206
16. Jaishankar M, Tseten T, Anbalagan N, Mathew BB, Beeregowda KN (2014) Toxicity, mechanism and health effects of some heavy metals. Interdiscip Toxicol 7:60
17. Tchounwou PB, Yedjou CG, Patlolla AK, Sutton DJ (2012) Heavy metal toxicity and the environment. Mol Clinic Environ Toxic 101:133–164
18. Sall ML, Diaw AKD, Gningue-Sall D, Aaron SE, Aaron JJ (2020) Toxic heavy metals: impact on the environment and human health, and treatment with conducting organic polymers, a review. Environ Sci Pollut Res 27:29927–29942
19. Lu H, Wang J, Stoller M, Wang T, Bao Y, Hao H (2016) An overview of nanomaterials for water and wastewater treatment. Adv Mater Sci Eng 2016
20. Sun L, Hu S, Sun H, Guo H, Zhu H, Liu M, Sun H (2015) Malachite green adsorption onto Fe_3O_4@ SiO_2-NH_2: isotherms, kinetic and process optimization. RSC Adv 5:11837–11844
21. Mahajan R, Chopda M (2009) Phyto-Pharmacology of Ziziphus jujuba Mill-A plant review. Pharmacogn Rev 3:320
22. Nazari M, Ghasemi N, Maddah H, Mousavi Motlagh M (2014) Synthesis and characterization of maghemite nanopowders by chemical precipitation method. J Nanostruct Chem 4:99
23. Miri A, Sarani M, Khatami M (2020) Nickel-doped cerium oxide nanoparticles: biosynthesis, cytotoxicity and UV protection studies. Rsc Adv 10:3967–3977
24. Malakotian M, Asadzadeh SN, Khatami M, Ahmadian M, Heidari MR, Karimi P, Firouzeh N. Varma RS (2019)) Protocol encompassing ultrasound/Fe_3O_4 nanoparticles/persulfate for the removal of tetracycline antibiotics from aqueous environments. Clean Technol Environ Policy 21:1665–1674
25. El Mendili Y, Bardeau J-F, Randrianantoandro N, Greneche JM, Grasset F (2016) Structural behavior of laser-irradiated γ-Fe_2O_3 nanocrystals dispersed in porous silica matrix: γ-Fe_2O_3 to α-Fe_2O_3 phase transition and formation of ε-Fe_2O_3. Sci Technol Adv Mater 17:597–609

26. Cao D, Li H, Pan L, Li J, Wang X, Jing P, Cheng X, Wang W, Wang J, Liu Q (2016) High saturation magnetization of γ-Fe_2O_3 nano-particles by a facile one-step synthesis approach. Sci Rep 6:1–9
27. Kim DS, Kwak S-Y (2007) The hydrothermal synthesis of mesoporous TiO_2 with high crystallinity, thermal stability, large surface area, and enhanced photocatalytic activity. Appl Catal A Gen 323:110–118
28. Takari A, Ghasemi AR, Hamadanian M, Sarafrazi M, Najafidoust A (2021) Molecular dynamics simulation and thermo-mechanical characterization for optimization of three-phase epoxy/TiO_2/SiO_2 nano-composites. Polym Test 93:106890
29. Najafidoust A, Hakki HK, Avalzali HA, Karimi Ashraf Bonab M (2019) The role of Diethanolamine as stabilizer in controlling morphology, roughness and photocatalytic activity of ZnO coatings in sonophotodegradation of methylene blue. Mater Res Exp 6:096401

Figures

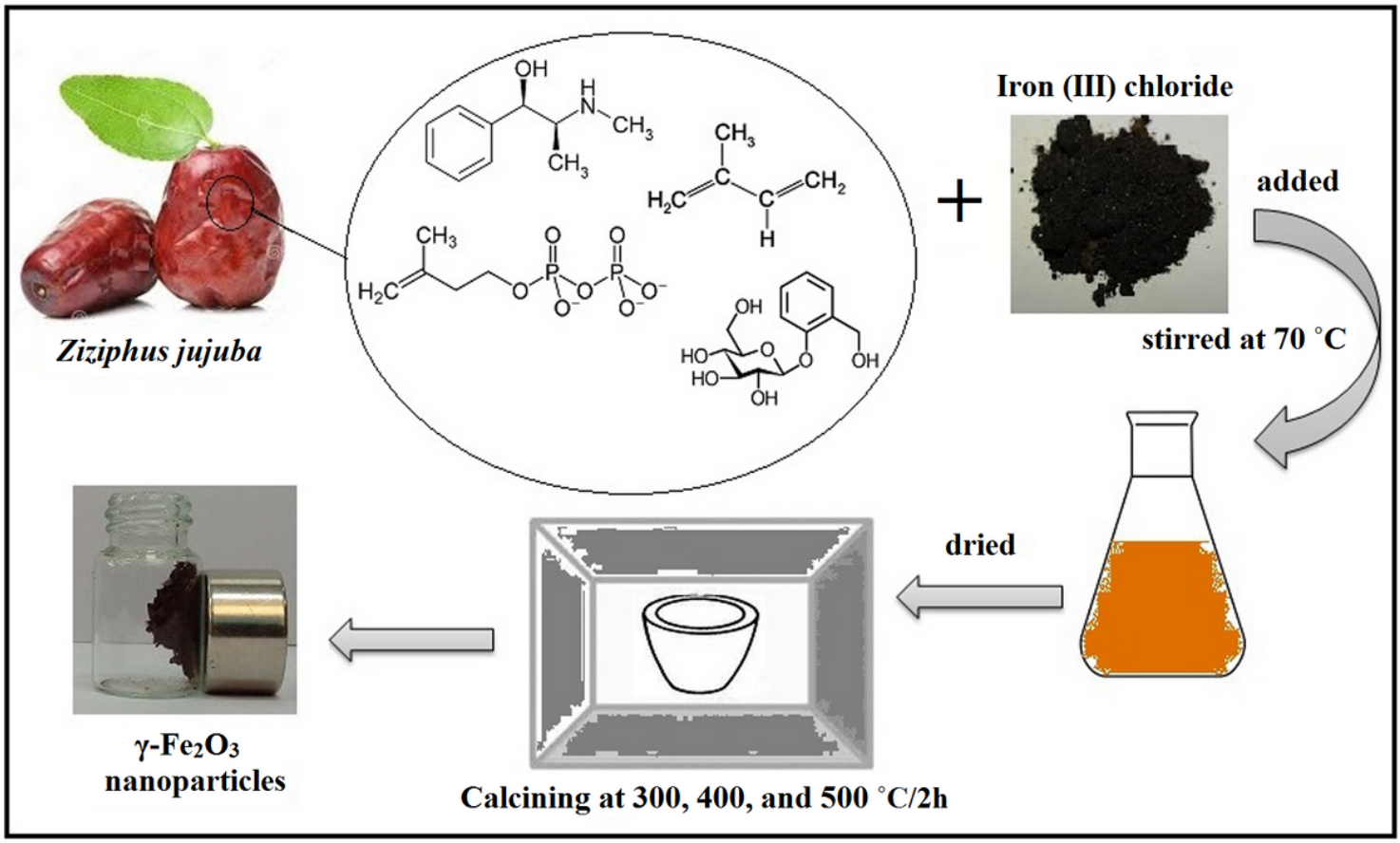

Figure 1

Schematic diagrams of the synthesis of γ-Fe2O3 NPs using extract of Z. jujuba fruit.

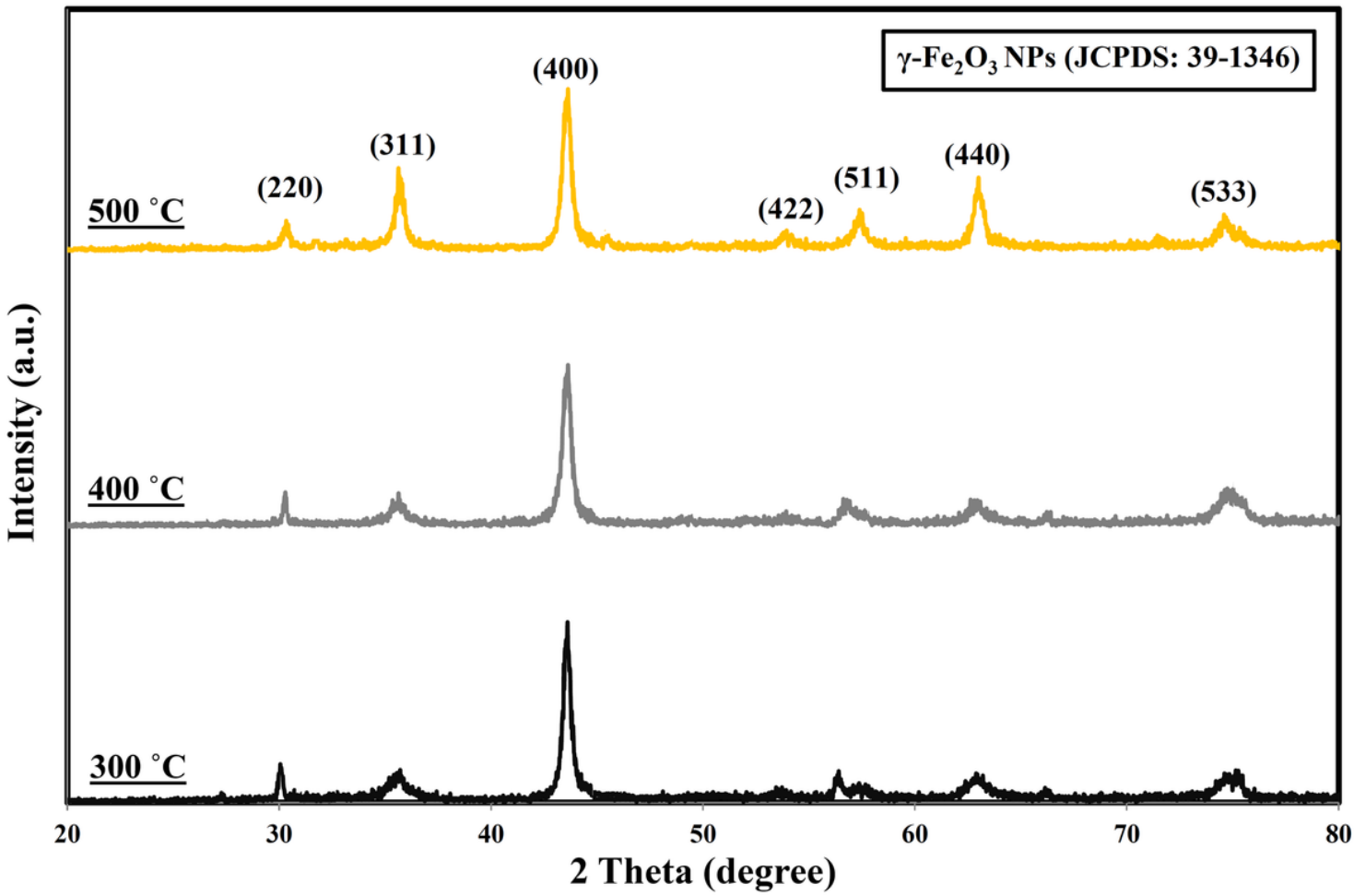

Figure 2

PXRD spectra of the synthesized γ-Fe2O3 NPs using aqueous extract of Z. jujuba at 300, 400 and 500 ˚C.

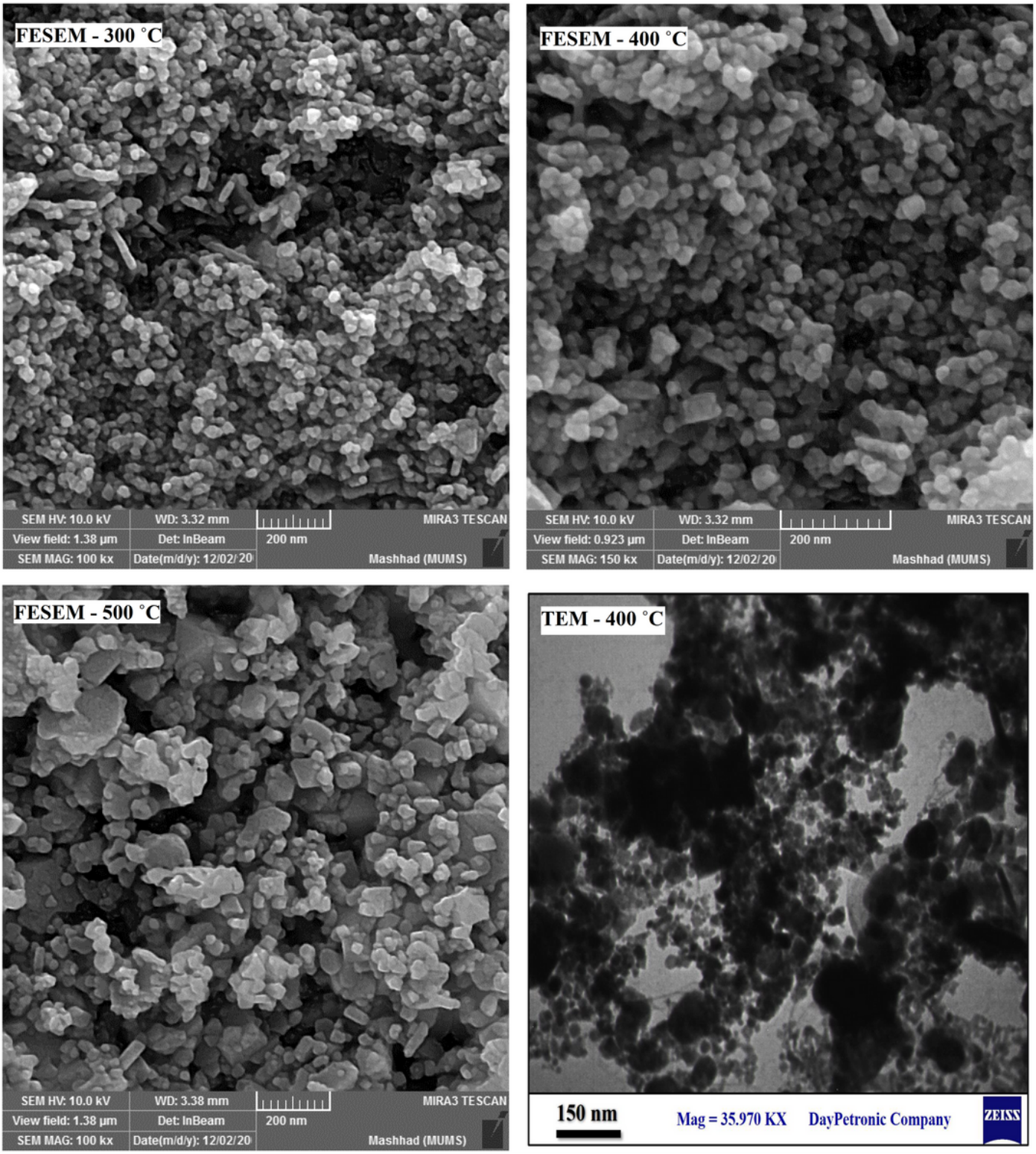

Figure 3

FESEM and TEM images of the synthesized γ-Fe2O3 NPs using aqueous extract of Z. jujuba at 300, 400, and 500 ˚C.

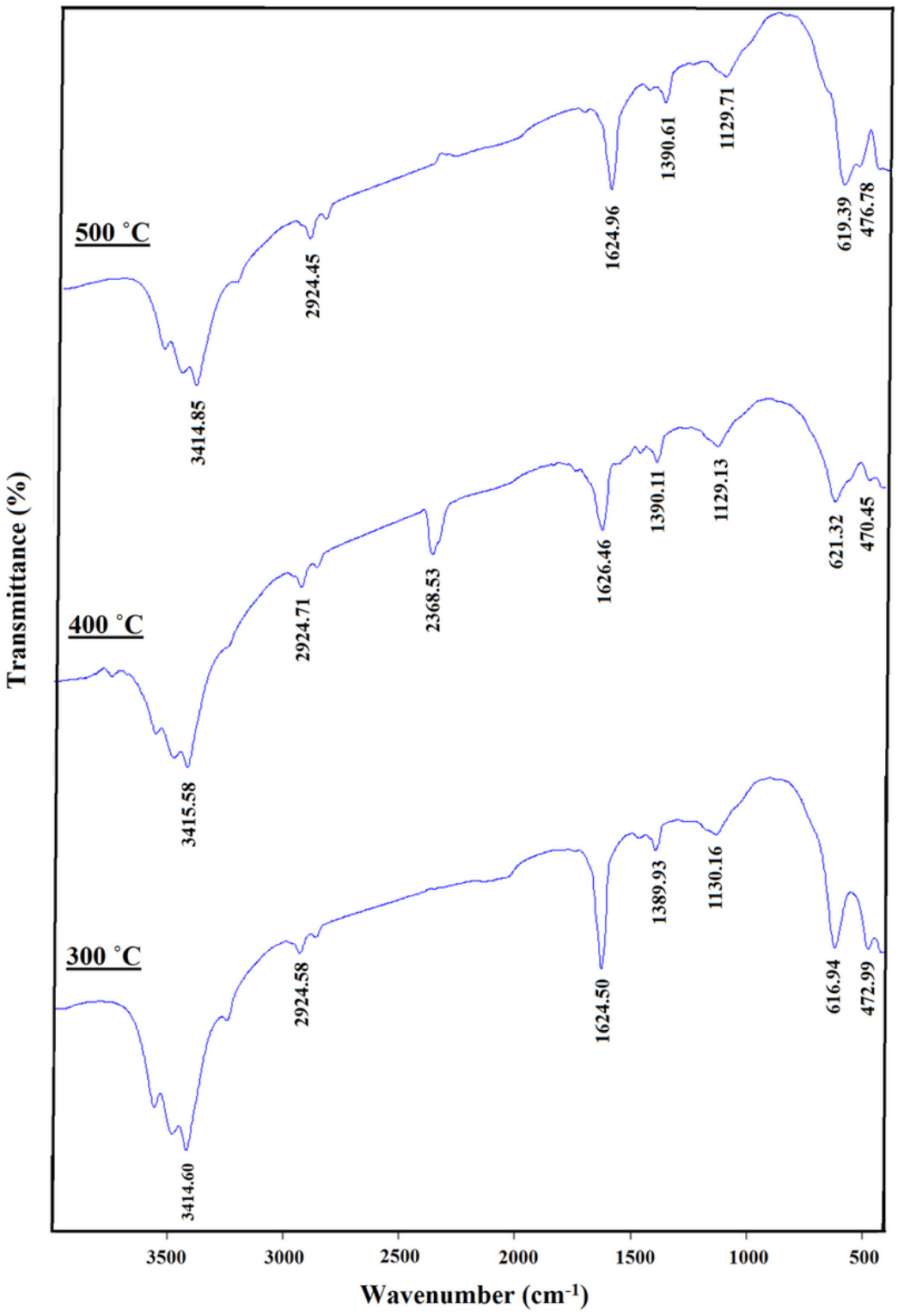

Figure 4

FT-IR spectra of the synthesized γ-Fe2O3 NPs using aqueous extract of Z. jujuba at 300, 400, and 500 ˚C.

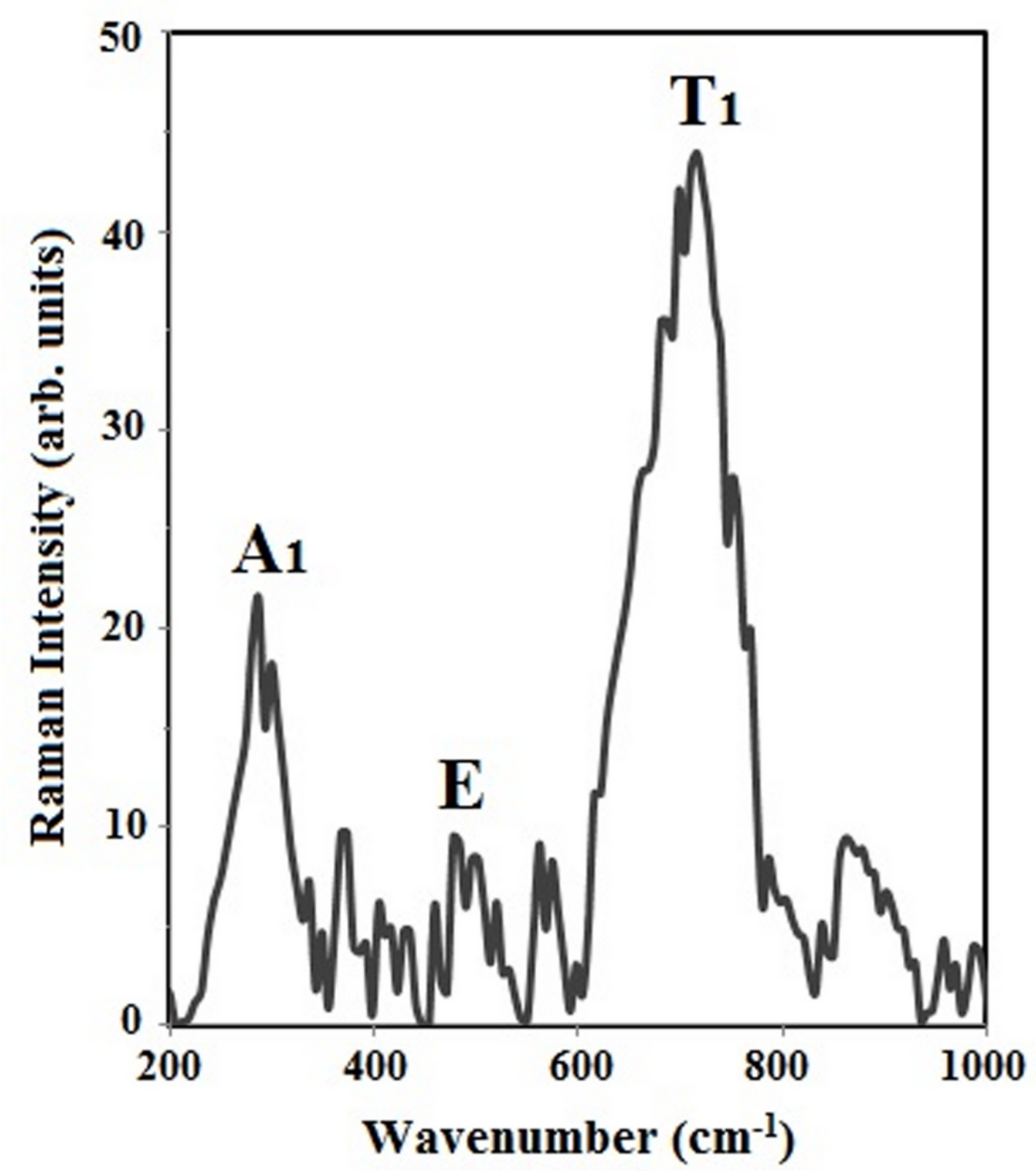

Figure 5

Raman spectrum of the synthesized γ-Fe2O3 NPs (at 400˚C) using aqueous extract of Z. jujuba.

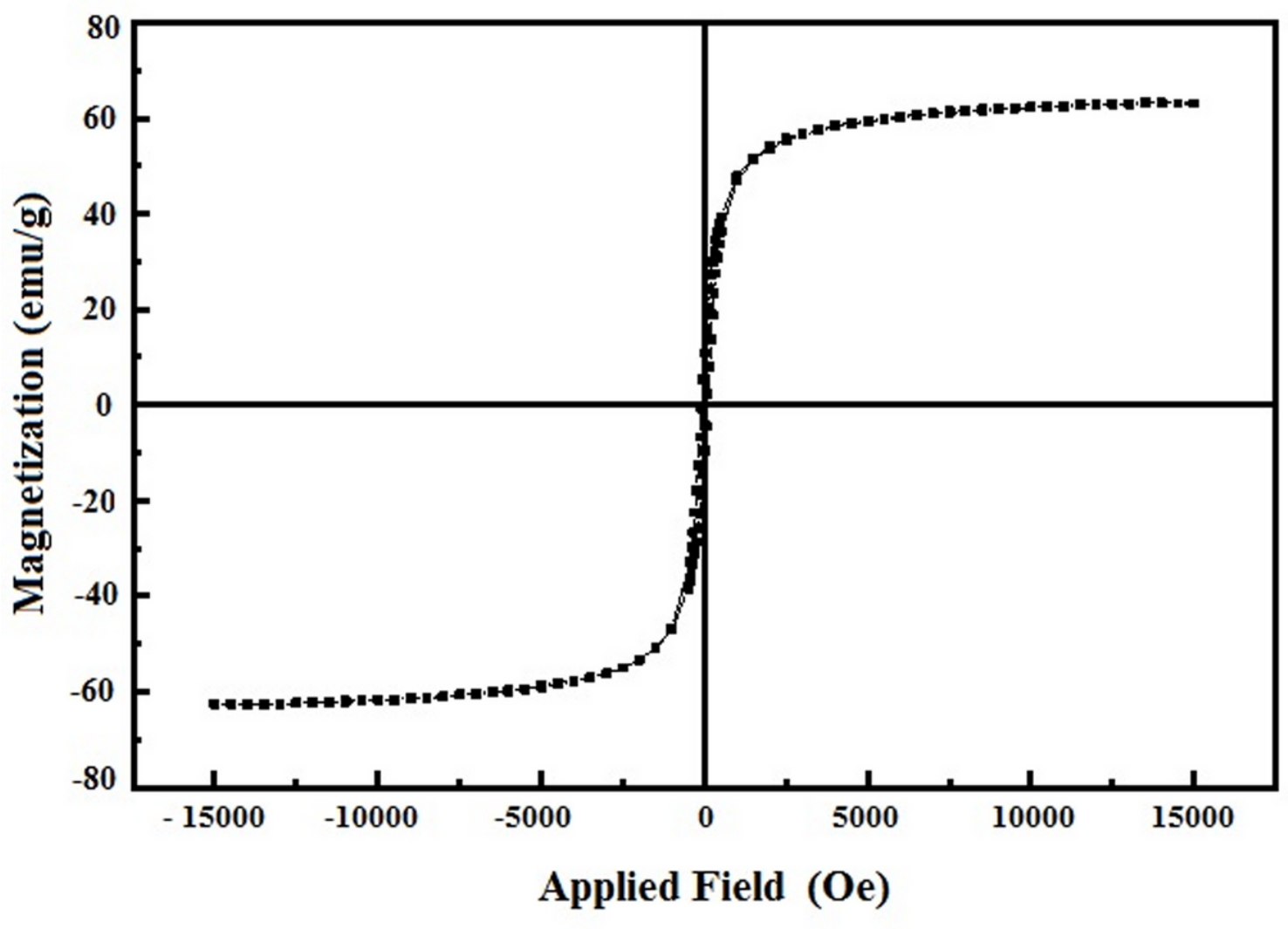

Figure 6

VSM graph of the synthesized γ-Fe2O3 NPs using aqueous extract of Z. jujuba.

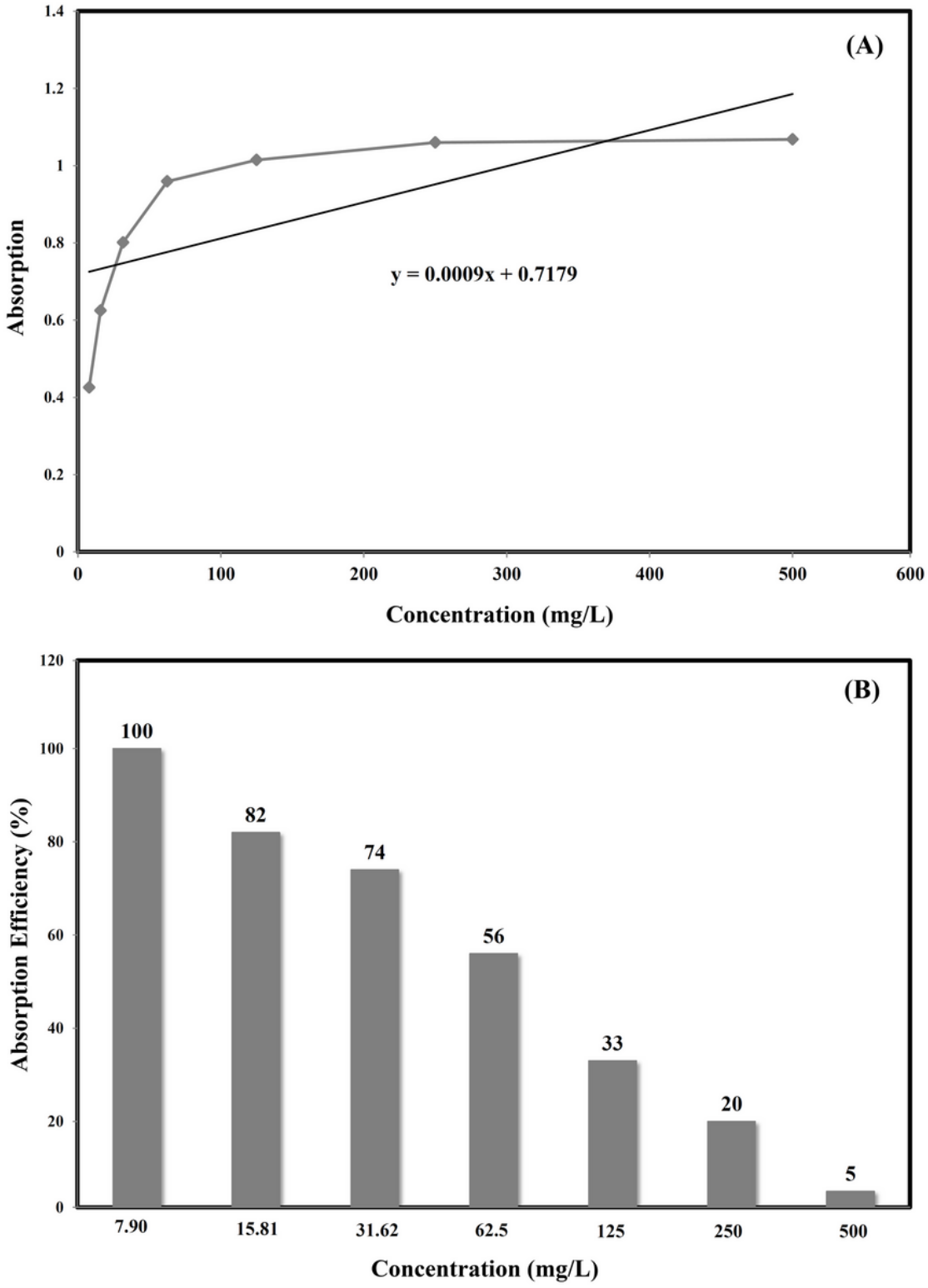

Figure 7

(A) Standard curve of lead absorption using synthesized γ-Fe2O3 NPs at 400 ˚C, (B) Adsorption efficiency of nanoparticles in different concentrations of lead at the pH of 8.

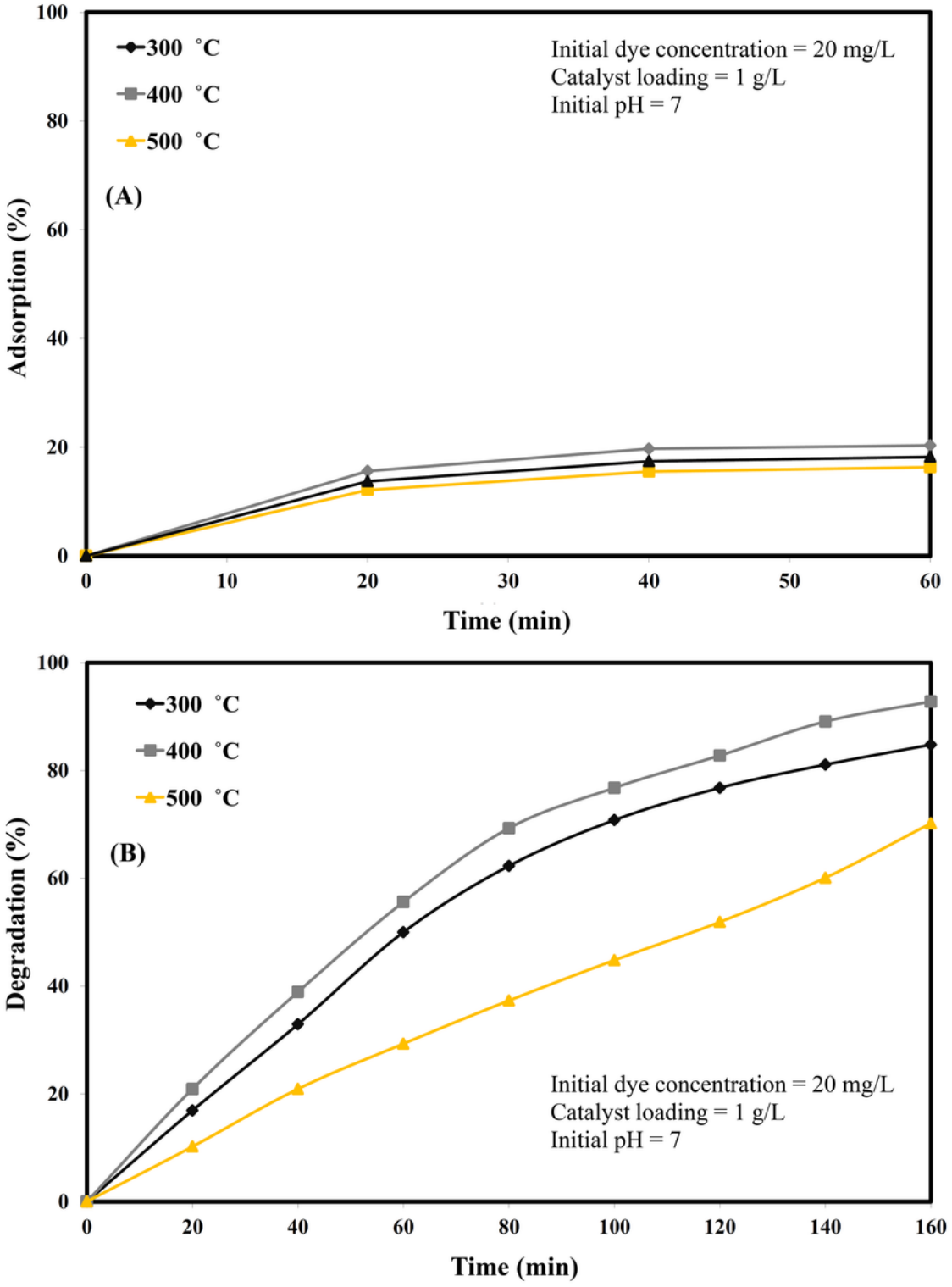

Figure 8

Photocatalytic degradation of MB using γ-Fe2O3 NPs under solar-light (A) adsorption and (B) degradation.

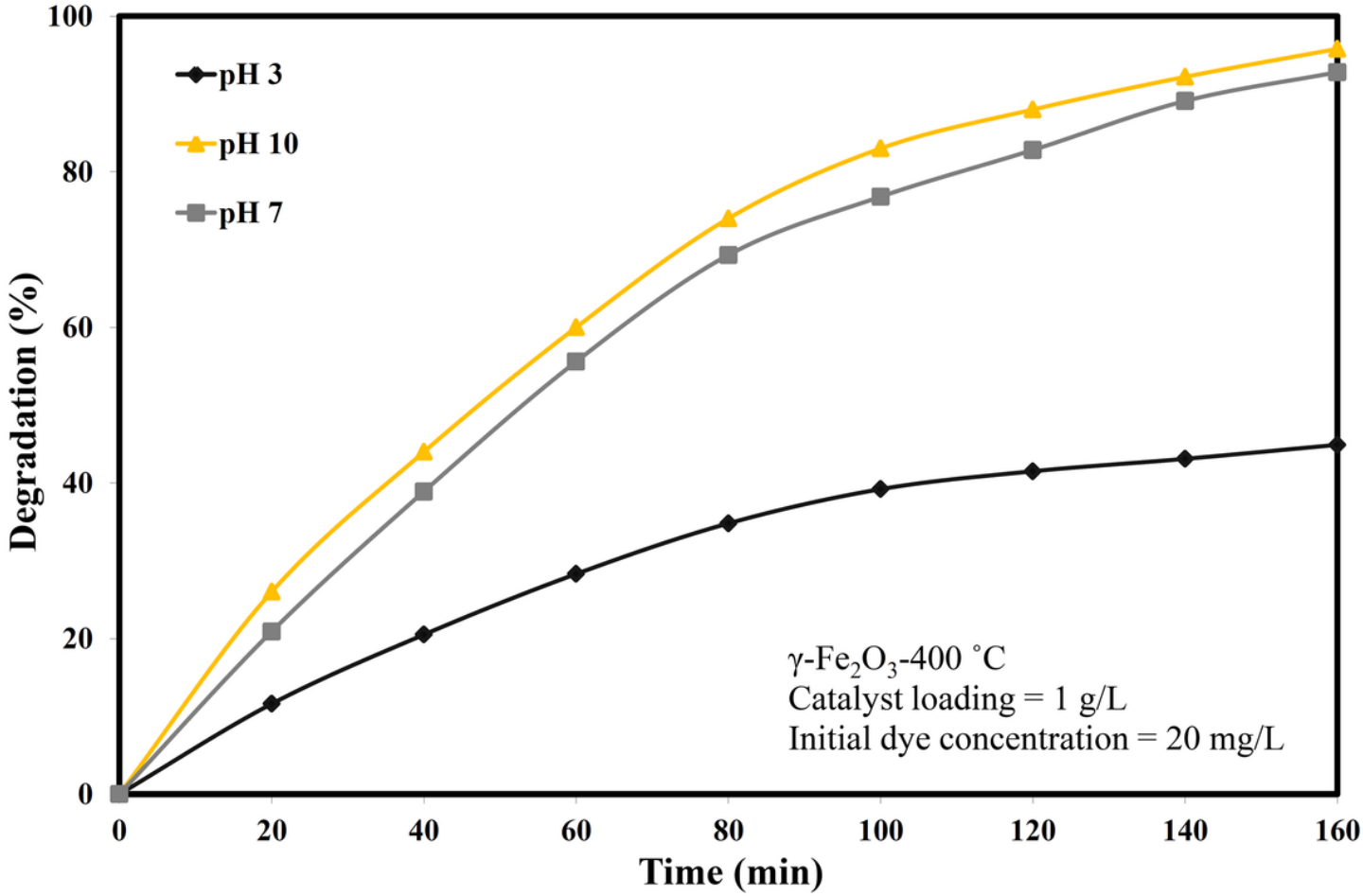

Figure 9

Influence of pH on photo-removal of methylene blue from wastewater using γ-Fe2O3 NPs at 400 ˚C.

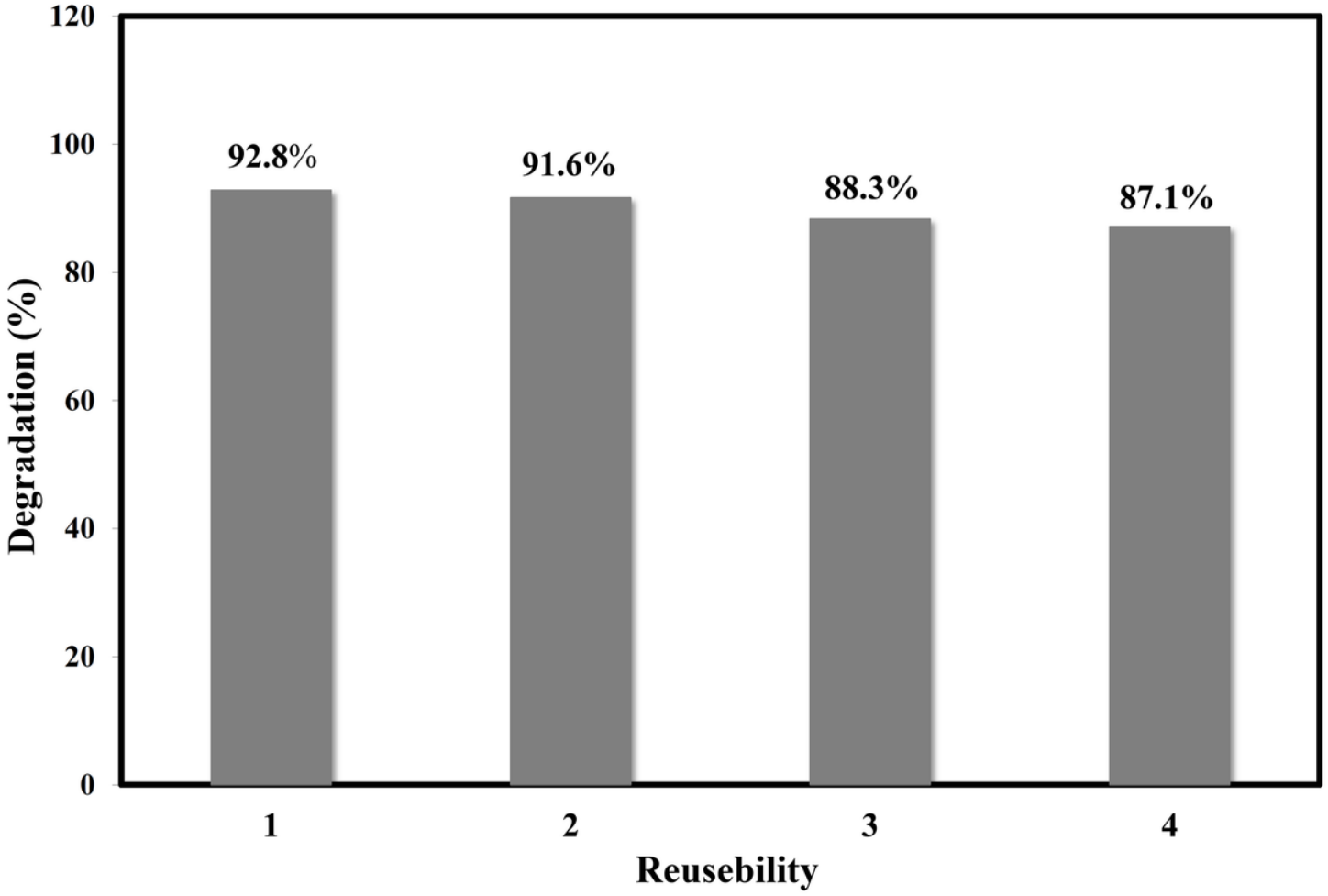

Figure 10

The reusability of synthesized γ-Fe2O3 NPs at 400 ˚C toward photo-degradation of methylene blue.